remote sensing

MDPI

Article

Application of Remote Sensing for Identifying Soil Erosion Processes on a Regional Scale: An Innovative Approach to Enhance the Erosion Potential Model

Siniša Polovina *, Boris Radić, Ratko Ristić and Vukašin Milčanović

Faculty of Forestry, University of Belgrade, Kneza Višeslava 1, 11030 Belgrade, Serbia; boris.radic@sfb.bg.ac.rs (B.R.); ratko.ristic@sfb.bg.ac.rs (R.R.); vukasin.milcanovic@sfb.bg.ac.rs (V.M.)
* Correspondence: sinisa.polovina@sfb.bg.ac.rs

Abstract: Soil erosion represents a complex ecological issue that is present on a global level, with negative consequences for environmental quality, the conservation and availability of natural resources, population safety, and material security, both in rural and urban areas. To mitigate the harmful effects of soil erosion, a soil erosion map can be created. Broadly applied in the Balkan Peninsula region (Serbia, Bosnia and Herzegovina, Croatia, Slovenia, Montenegro, North Macedonia, Romania, Bulgaria, and Greece), the Erosion Potential Method (EPM) is an empirical erosion model that is widely applied in the process of creating soil erosion maps. In this study, an innovation in the process of the identification and mapping of erosion processes was made, creating a coefficient of the types and extent of erosion and slumps (φ), representing one of the most sensitive parameters in the EPM. The process of creating the coefficient (φ) consisted of applying remote sensing methods and satellite images from a Landsat mission. The research area for which the satellite images were obtained and thematic maps of erosion processes (coefficient φ) were created is the area of the Federation of Bosnia and Herzegovina and the Brčko District (situated in Bosnia and Herzegovina). The Google Earth Engine (GEE) platform was employed to process and retrieve Landsat 7 Enhanced Thematic Mapper plus (ETM+) and Landsat 8 Operational Land Imager and Thermal Infrared Sensor (OLI/TIRS) satellite imagery over a period of ten years (from 1 January 2010 to 31 December 2020). The mapping and identification of erosion processes were performed based on the Bare Soil Index (BSI) and by applying the equation for fractional bare soil cover. The spatial–temporal distribution of fractional bare soil cover enabled the definition of coefficient (φ) values in the field. An accuracy assessment was conducted based on 190 reference samples from the field using a confusion matrix, overall accuracy (OA), user accuracy (UA), producer accuracy (PA), and the Kappa statistic. Using the confusion matrix, an OA of 85.79% was obtained, while UA ranged from 33% to 100%, and PA ranged from 50% to 100%. Applying the Kappa statistic, an accuracy of 0.82 was obtained, indicating a high level of accuracy. The availability of a time series of multispectral satellite images for each month is a crucial element in monitoring the occurrence of erosion processes of various types (surface, mixed, and deep) in the field. Additionally, it contributes significantly to decision-making, strategies, and plans in the domain of erosion control work, the development of plans for identifying erosion-prone areas, plans for defense against torrential floods, and the creation of soil erosion maps at local, regional, and national levels.

Keywords: soil erosion; land degradation; erosion potential method; remote sensing; Landsat; Google Earth Engine; bare soil index

Citation: Polovina, S.; Radić, B.; Ristić, R.; Milčanović, V. Application of Remote Sensing for Identifying Soil Erosion Processes on a Regional Scale: An Innovative Approach to Enhance the Erosion Potential Model. *Remote Sens.* **2024**, *16*, 2390. https://doi.org/10.3390/rs16132390

Academic Editors: Nikolaos L. Tsakiridis, Uta Heiden, Nikolaos Tziolas and Lenio Soares Galvao

Received: 4 April 2024
Revised: 5 June 2024
Accepted: 26 June 2024
Published: 28 June 2024

1. Introduction

Soil erosion represents a major global exacerbator of the degradation of land and water resources. Wind and water are dominant drivers of degradation, with particular attention in this regard paid to water erosion [1]. Considering both variable and non-variable groups

of parameters (temporally static and temporally dynamic parameters), agricultural lands and degraded forests are more sensitive to the occurrence and intensity of erosion processes than grassland areas [2,3]. Numerous studies and projects indicate that anthropogenic activity is the leading cause of changes in land use patterns [4–8]. Besides anthropogenic factors, changes in land use are influenced by natural factors such as lithology, hydrology, topography, climate, and pedology [9,10].

Soil loss caused by erosion represents a significant global, regional, and Balkan Peninsula-wide issue. Therefore, it is necessary to conduct the spatial identification and quantification of soil loss, serving as a prerequisite for the sustainable management of vital environmental resources. Accordingly, modeling represents a significant procedure for obtaining essential information necessary for understanding the occurrence of erosion processes and assessing soil loss.

In Europe, the dominant form of erosion is rainfall erosion, while wind erosion occurs to a lesser extent. Water erosion is most prevalent in Southern Europe but is also increasingly becoming a problem in Northern Europe [11]. In pertinent documents, the European Union has recognized that erosion processes are one of the main factors contributing to land degradation [12], causing material damage amounting to several billion euros annually [13]. The European Commission's Thematic Strategy for Soil [12] proposed using models to monitor erosion processes [14–17]. Erosion modeling is based on understanding nature's physical laws and processes. By applying models, natural methods are described using mathematical formulations [18]. Erosion models involve the simplification (streamlining) of processes in reality, with one of the goals being the determination of the essential factors and segments [19]. With the advancement of technology and software tools, models can now be categorized into empirical, conceptual, and physically based types [20,21]. Authors such as Hajigholizadeh et al. [22] have proposed forming so-called "hybrid" models that combine all these concepts. RUSLE represents an empirical model that has the widest application worldwide and uses quantified and verified high-resolution input data [14,17,23]. Application of the RUSLE2015 model has revealed that the average soil loss in European Union countries amounts to 2.46 $t \cdot ha^{-1} \cdot year^{-1}$, resulting in a total soil loss of 970 Mt annually [14]. To ensure that the produced soil erosion map is compatible with the traditional approach used in the countries of the Balkan Peninsula over the past few decades, and which allows for comparison with previously created soil erosion maps for the purpose of determining changes in erosion potential over recent decades, it was necessary to use the Erosion Potential Method (EPM). However, the traditional approach of this method was characterized by an outdated perception of land degradation and the use of analog databases, and as such, it did not meet contemporary standards. In the countries of the former Yugoslavia, the EPM has been utilized for the past 50 years [24–27]. This method has been extensively applied in all the former Yugoslavian states, namely, Bosnia and Herzegovina [28], North Macedonia [29,30], Montenegro [31], Croatia [32,33], and Slovenia [34–36], as well as in Germany [37], Italy [38–40], Argentina [41], Belgium [20], Greece [42–45], Algeria [46], Morocco [47,48], Iraq [49], Iran [50], Brazil [51,52], Chile [53], and Colombia [54]. Gross and net soil erosion rates have been assessed globally using the original model (EPM) and its modified version (mEPM) [55]. The EPM is based on the analytical processing of data on the factors that influence erosion, such as climatic characteristics (temperature and precipitation), soil erodibility, land use and land cover, slope, and the type, extent, and intensity of erosion processes. One of the basic parameters used in calculating soil erosion intensity is the coefficient of the types and extent of erosion and slumps (φ). According to the original version of the EPM [24], this coefficient (φ) is determined directly in the field. In order to obtain relevant data on the coefficient of visible and clearly expressed erosion processes, it is necessary to determine the visible manifestations (traces) of erosion processes and define the boundaries of the areas where such processes occur. This is a demanding process that requires detailed and comprehensive field research.

The aim of conducting field research, or surveying the torrential bed and watershed area or erosion zone, is to understand the type, extent, and intensity of erosion processes. It is necessary to assess the condition of the bottom and banks of a torrential bed and the characteristics of sediments and observe occurrences of slope wash, land sliding, bank undercutting, and other destructive processes. Crucial to this endeavor is the identification of unvegetated and neglected areas, all constituting erosion processes that may be of deep, mixed, and surface types: gullies; scree, sheet, rill, and gully erosion; sinkholes; landslides; and fissures [24,56]. Identifying areas covered with sterile sediment, barren land, and rocky regions is essential. It is of vital importance to determine the pertinent spatial structure, which includes organic surfaces exposed to soil deflation, degraded forests and thickets, "unstable" land (with traces of solifluction and shallow landslides), surfaces exposed to sedimentation from torrential beds, and the precise dimensions of cross profiles, which reveal the movement of sediments. It is also crucial to identify and spatially map soil erosion in forested areas, where many hidden erosion processes occur and are not visible based on aerial photographs due to the density of the canopy and vegetation [24,26].

In line with the mentioned issues in research and engineering practice, there is an evident potential for the application of modern technologies and software tools in a Geographic Information System (GIS) environment using remote sensing (RS) techniques, which will expedite the process of identifying and mapping erosion processes as well as estimating soil loss due to water erosion.

RS techniques offer invaluable tools for monitoring and assessing environmental changes, including soil erosion, in various areas. RS techniques encompass a wide range of methods and technologies that allow the collection of information about the Earth's surface and atmosphere from a distance. These techniques use sensors mounted on airplanes or satellites to capture electromagnetic radiation reflected or emitted by the Earth's surface [57]. By analyzing these data, researchers can gain valuable insights into soil erosion processes, identify vulnerable areas, and provide information for land management strategies. Numerous methodologies based on RS have been developed to address the challenges of identifying areas susceptible to extensive soil erosion. These methodologies involve the use of different types of RS data, including optical, thermal, and radar images, as well as Light Detection and Ranging (LiDAR) data, to characterize the properties of land surfaces associated with erosion risk [58–61].

To date, several different methods for soil erosion identification and terrain susceptibility assessment have been developed, particularly with the increasing use of GIS and satellite imagery containing various spectral bands [15–17]. The first methods for soil erosion identification and mapping were developed at the pixel level [62], and they involved assigning an individual pixel to a specific class [63]. In pixel-based classification, it is assumed that each pixel corresponds to a single homogeneous type of soil erosion; however, many pixels capture multiple different types. This assumption led to the development of sub-pixel classification to address the anomalies in classifying the soil erosion types of mixed pixels [64].

Spectral indices represent the next step in the development of RS techniques for mapping and predicting soil erosion processes, emerging with the development of satellites containing various spectral bands. To create spectral indices, arithmetic operations and empirical relationships are applied, allowing the modification or combination of original spectral bands into new images, thereby clearly determining specific characteristics in an image [57]. Singh et al. [65] established a relationship between soil color and the normalized difference vegetation index (NDVI) using National Oceanic and Atmospheric Administration (NOAA)/Advanced Very-High-Resolution Radiometer (AVHRR) data. Using satellite images with a coarse spatial resolution of 1.1 km, they identified erosion processes and mapped eroded soils that resulted from the removal of the topsoil layer and a subsequent reduction in the amount of organic matter [65].

The increased availability of high-spatial-resolution satellite imagery has provided opportunities for the creation of numerous new methods for mapping, identifying, and

predicting soil erosion. As a result, methods based on object-based image analysis (OBIA) have been developed [66]. OBIA does not involve using individual pixels as the basic unit for classification; instead, it involves the analysis of groups of pixels, i.e., objects, which are classified accordingly [67]. This approach reduces intra-class variation and eliminates impulse noise, which arises from isolated pixels, in an image, with the latter mainly occurring due to misclassification [68]. Objects are created in the segmentation process, wherein pixels are grouped based on similar spectral characteristics, shapes, and textures relative to neighboring elements and objects [69]. OBIA has been widely applied in mapping gully systems and identifying their changes over time, processes crucial for implementing soil conservation measures [70,71]. Advances in pattern recognition techniques and methods, in which artificial intelligence and machine learning are applied, have resulted in significant developments in the new generation of techniques for the identification and mapping of erosion processes and predicting soil erosion, such as support vector machines (SVMs), Random Forest (RF) methods, artificial neural networks (ANNs), and decision trees [72–75].

The general aim of this research was to develop an approach suitable for mapping the intensity of erosion processes and identifying the corresponding coefficient (φ), which represents one of the sensitive parameters in the EPM model. Specifically, our objectives were to (1) identify erosion processes and map their forms using RS techniques; (2) expedite fieldwork, especially for large areas such as the territory of Bosnia and Herzegovina (BiH); and (3) create a soil erosion map and a sediment production map to allow appropriate measures to be taken to mitigate soil erosion issues. The novel contribution of this research is the development of an innovative approach to the application of the EPM, which has been used in the Balkan Peninsula for over half a century and continues to be refined. To overcome the discussed limitation, this work consists of guidelines for determining the value of the coefficient of the types and extent of erosion and slumps (φ) using multispectral satellite images obtained via RS methods, as well as using spectral indices that represent the primary products of spectral bands.

2. Materials and Methods

2.1. Study Area

The Federation of Bosnia and Herzegovina (FBiH) and the Brčko District (BD), along with Republika Srpska (RSR), together constitute the state of Bosnia and Herzegovina (BiH), located in Southeastern Europe, geographically belonging to the Adriatic and Black Sea watersheds, specifically to the group of Mediterranean and Danubian countries. It is located in the central part of the Balkan Peninsula (Figure 1), between latitude 42°26′N and 45°15′N and longitude 15°45′E and 19°41′E. Bosnia and Herzegovina covers an area of 51,209.2 km^2, while the researched area of the FBiH and the BD covers an area of 26,570 km^2.

The relief of BiH is predominantly hilly–mountainous, but at the same time, it is also highly dissected by valleys along major rivers. This area's geological structure is exceptionally complex, resulting in diverse rock formations (magmatic, sedimentary, metamorphic, and many transitional forms) [76,77]. Three climate zones are represented in the territory of BiH: Mediterranean, Alpine, and Central European climates [77]. Regarding soil types, the most prevalent are calcomelanosol, district cambisols, and calcocambisols in the hilly–mountainous region. Among the automorphic soil types in the hilly–mountainous region, lithosols, regosols, red soils, rendzinas, luvisols, podzols, and smonits are represented [76]. Some hydromorphic soils, such as pseudogleys and fluvisols, which are the most common, are present in lowland areas [77]. According to Corine Land Cover 2018 [78], the majority of the territory of BiH is covered by forests (53.2%), while agriculture occupies 26.8% of the land. Urban and transportation areas together account for 1.7% of the total land.

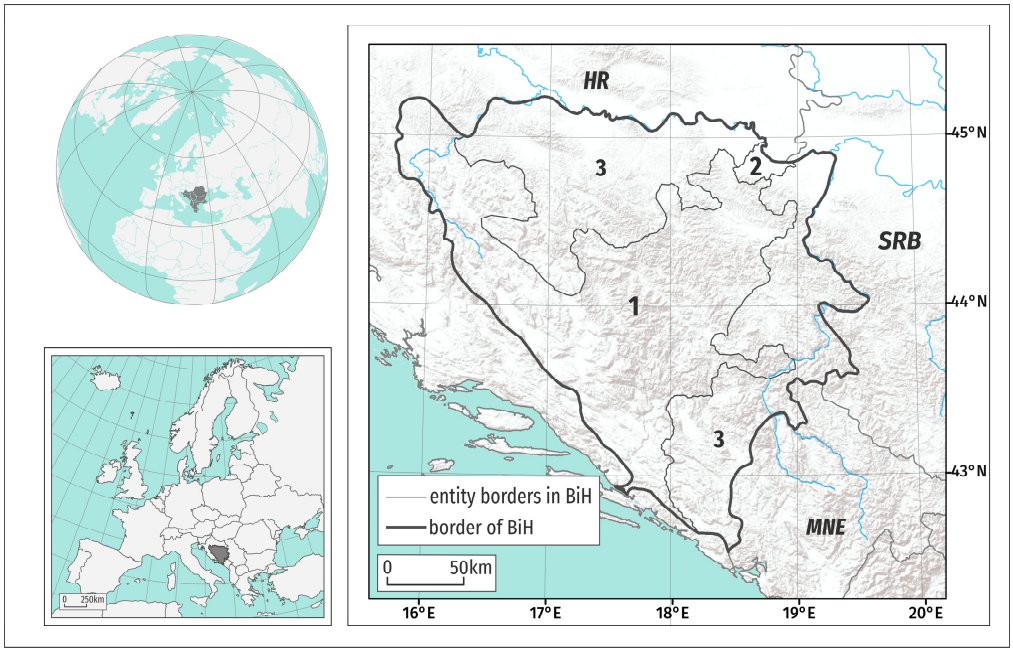

Figure 1. Study area: 1—the Federation of Bosnia and Hercegovina (FBiH); 2—the Brčko District (BD); 3—the Republic of Srpska (RSR); BiH—Bosnia and Hercegovina; SRB—Serbia; MNE—Montenegro; HR—Croatia.

2.2. Erosion Potential Method (EPM)

The EPM is an empirical method for assessing soil loss, erosion production, and sediment transport in a watershed, erosion area, or land parcel. This technique was developed based on long-term field research, observations, and watershed measurements [24,27]. In addition to calculating sediment production and transport, this method was designed for mapping erosion processes in erosion-prone areas and quantitatively classifying torrential flows [24–26]. This method is a standard tool for solving engineering problems related to preventing soil erosion and torrential floods in water management. To develop water management foundations, studies, and projects, Equation (1) is used [20]:

$$W_{year} = T \cdot H_{year} \cdot \pi \cdot \sqrt{Z^3} \cdot A \quad (1)$$

W_{year}—Total production of erosive material [$m^3 \cdot year^{-1}$]; T—temperature coefficient [-]; H_{year}—mean annual precipitation [mm]; π—3.14; Z—coefficient of erosion [-]; A—watershed area [km^2].

The method starts with the analytical processing of data on factors influencing erosion. Since erosion is a spatial phenomenon, it is represented on maps based on classification according to the analytically calculated erosion coefficient (Z), which is not dependent on climatic characteristics but on soil characteristics, vegetation cover, relief, and the visible occurrence of erosion processes. The erosion coefficient (Z) is obtained from Equation (2) [24]:

$$Z = Y \cdot X \cdot a \cdot \left(\varphi + \sqrt{I_{mean}}\right) \quad (2)$$

Z—Erosion coefficient [-]; Y—soil erodibility coefficient (soil resistance to erosion) [-]; X·a—soil protection coefficient (land use and land cover) [-]; φ—coefficient of type and extent of erosion and slumps [-]; I_{mean}—the mean slope of the terrain [%].

Based on the erosion coefficient Z, erosion processes can be categorized according to the work by Gavrilović (Table 1). The values typically range from 0.1 to 1.5 and higher, i.e., from preserved, mildly eroded catchments and areas to catchments significantly degraded due to soil erosion. Z values may only be above and below the mentioned thresholds

in exceptional cases [24]. Thirteen categories have been established based on the type of prevailing erosion and the values of the erosion coefficient Z [24].

Table 1. Classification of the erosion classes according to the Z coefficient [24].

Erosion Category	Intensity of Erosion Processes	Dominant Erosion Type	Erosion Coefficient Z	Mean Value of Z
I	Excessive erosion	Deep	>1.51	1.25
		Mixed	1.21–1.50	
		Surface	1.01–1.20	
II	Severe erosion	Deep	0.91–1.00	0.85
		Mixed	0.81–0.90	
		Surface	0.71–0.80	
III	Medium erosion	Deep	0.61–0.70	0.55
		Mixed	0.51–0.60	
		Surface	0.41–0.50	
IV	Slight erosion	Deep	0.31–0.40	0.30
		Mixed	0.25–0.30	
		Surface	0.20–0.24	
V	Very slight erosion	Traces of erosion	0.01–0.19	0.10

The soil erodibility coefficient (Y) depends on the climatic conditions of the environment, geological substrate, and types of pedological formations being analyzed. According to the original method, the values of the coefficient range from 0.25 for bare and compact rocks to 2.0 for fine sediments and unbound soils without the ability to resist erosion [24].

The soil protection coefficient (X·a) relates to the soil's protection from atmospheric agents and erosion effects. This coefficient comprises the original or 'unchanged' land cover ('X') and soil protection measures ('a'). According to Gavrilović, its values range from 0.05 to 1.0 [24].

The mean slope of the terrain (Imean) reflects the influence of topographic characteristics, utilizing the square root of the mean slope of the watershed, erosion area, or land parcel [24].

The coefficient of the types and extent of erosion and slumps (φ) represents the numerical equivalent of visible and clearly expressed erosion processes in a watershed or erosion area (Table 2). According to the original method, the factor values range from 0.1 (areas without visible signs of erosion) to 1.0 (areas affected by deep erosion) [24].

One of the fundamental parameters for calculating soil erosion intensity is the coefficient of the types and extent of erosion and slumps (φ). According to the original version of the EPM [24], the coefficient of the types and extent of erosion and slumps (φ) is determined directly in the field. To obtain relevant data on the coefficient of the types and extent of erosion, it is necessary to determine the visible manifestations (traces) of erosion processes and the boundaries of the areas affected by such processes. The coefficient of the types and extent of erosion and slumps (φ) is the only parameter in the EPM with a subjective element, greatly distancing it from the attribute of being 'empirical'. For this reason, De Vente and Poesen [20] classify this method as 'semi-quantitative'. To overcome this limitation, this study consists of guidelines for determining the values of the coefficient of the type and extent of erosion and slumps (φ) using multispectral satellite imagery obtained through RS and spectral indices representing primary products of spectral channels. The obtained values of the coefficient of the types and extent of erosion and slumps in the researched areas of the FBiH and the BD were verified in the field, where the validation and accuracy assessment of the thematic maps obtained were performed (Figure 2).

Table 2. Basic characteristics φ coefficient according to the EPM model [24].

φ Description—Type and Extent of Erosion and Slumps	φ Value
Watershed completely under gully erosion and primordial processes (deepening, incision, slumps)	1.0
About 80% of the watershed is under furrow and gully erosion	0.9
About 50% of the watershed is under furrow and gully erosion	0.8
The entire watershed is subject to surface erosion: disintegrated debris from embankments, some furrows, and gullies, as well as strong karst erosion	0.7
The entire watershed is under surface erosion but without furrows and gullies (deep processes) and the like	0.6
Land with 50% of the area covered by surface erosion, while the rest of the watershed is preserved	0.5
Land with 20% of the area covered by surface erosion, while 80% of the watershed is preserved	0.3
The soil in the watershed has no visible signs of erosion, but there are minor slips and slides in watercourses	0.2
Watershed without visible signs of erosion, but mostly under arable land	0.15
An area without visible signs of erosion, both in the watershed and in the watercourses, but predominantly under forests and perennial vegetation (meadows, pastures, etc.)	0.1

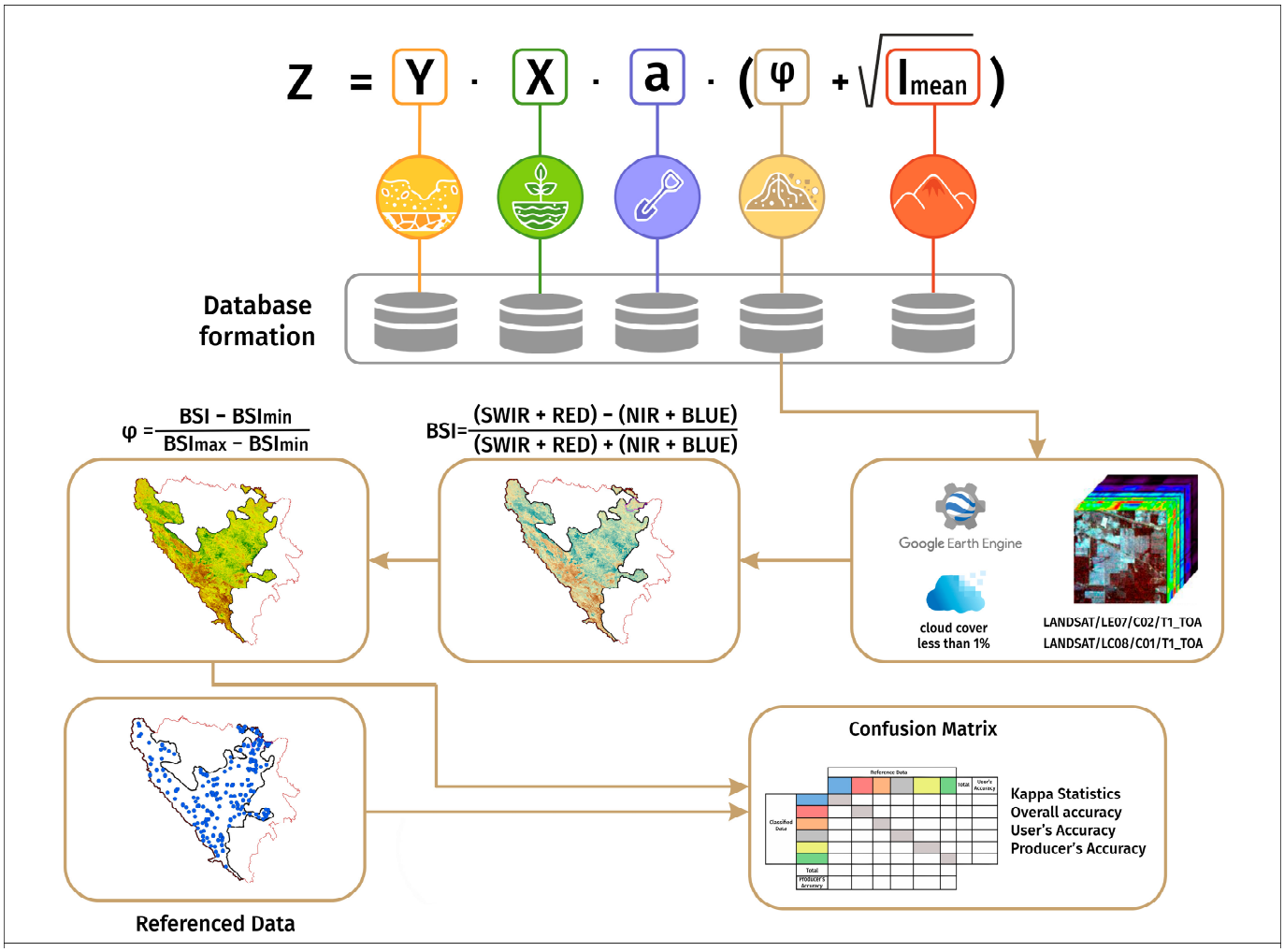

Figure 2. Workflow using remote sensing in the calculation of the coefficient of type and extent of erosion and slumps (φ). Note: Z—Erosion coefficient; Y—soil erodibility coefficient; X—land cover coefficient; a—soil protection measures coefficient; Imean—the mean slope of the terrain; BSI—the bare soil index.

2.3. Application of Multispectral Satellite Imagery

The initial step in determining the φ coefficient involves using multispectral satellite imagery obtained through RS methods and applying geostatistical processes and tools in GIS environments while using ArcMap 10.8.2 [79] software to process satellite images and obtain the spectral BSI.

Based on the obtained spectral BSI, field investigation work is conducted to validate and calibrate the obtained parameters and assess the accuracy of the results. Depending on the research objectives, financial capabilities, and the characteristics of the sensors themselves, satellite imagery from state and private institutions and companies is used, with the imaging results being available either free of charge or commercially. The need to model and identify erosion processes based on satellite imagery depends on the user needs, research objectives, and the scope of a project, as well as the spatial and temporal resolution requirements of the satellite image.

To perform the mapping and identification of erosion processes, spectral indices were used, representing primary products generated from multispectral satellite imagery from Landsat Missions 7 and 8. The Landsat Mission 7 satellite utilizes the ETM+ sensor, with 7 spectral channels with spatial resolutions of 30 m and 120 m and a panchromatic channel with a spatial resolution of 15 m. The Landsat Mission 8 satellite carries two types of sensors: an OLI and a TIRS. Both sensors have 11 spectral channels with spatial resolutions of 15 m (a panchromatic channel), 30 m (8 channels), and 100 m (2 channels).

The initial phase of this study involved collecting satellite images obtained through RS in Landsat satellite missions; these images were acquired using the Google Earth Engine (GEE) platform. The GEE is an advanced cloud-based computational platform designed for processing and analyzing Earth Observation (EO) data [80,81].

To create a thematic map representing the coefficient of the types and extent of erosion and slumps (φ) for the territories of the FBiH and the BD, satellite images were collected for 10 years (from 1 January 2010 to 31 December 2020). Before they were downloaded, the digital processing of the images was performed. The analysis and processing of the digital images consisted of using specific mathematical operations, functions, and algorithms such as image preprocessing, image enhancement, and image transformation. Satellite images were used, with an atmospheric correction of Landsat 7 Collection 2 Tier 1 Top of the Atmosphere (TOA) Reflectance ("LANDSAT/LE07/C02/T1_TOA") and Landsat 8 Collection 1 Tier 1 Top of the Atmosphere (TOA) Reflectance ("LANDSAT/LC08/C01/T1_TOA") [82]. The next step in the GEE application involves setting input parameters for maximum cloud cover in image tiles and the region of interest (ROI), targeting nearly clear-sky conditions with less than 1% cloud cover. Satellite images were used in vegetative and non-vegetative periods to obtain more relevant results. In total, 648 cloud-free satellite images were used: Landsat 7 Collection 2 Tier 1 TOA Reflectance (344 products) and Landsat 8 Collection 1 Tier 1 TOA Reflectance (304 products). The original data were supplied as projected in the WGS84/UTM zone 34N coordinate system.

The algorithm used for the geospatial processing and downloading of the Landsat satellite images and the Bare Soil Index (BSI) using the GEE platform is shown in Figure 3. In the first step, five different input parameters are required: the start and end dates of the images (allowing the selection of the desired time frame); the collection of images from different Landsat missions, allowing the maximum cloud cover in an image; and the region of interest for which the images are processed. The next step involves the transformation of the satellite images based on spectral channels to obtain the BSI and the procedure for downloading the thematic map onto a computer.

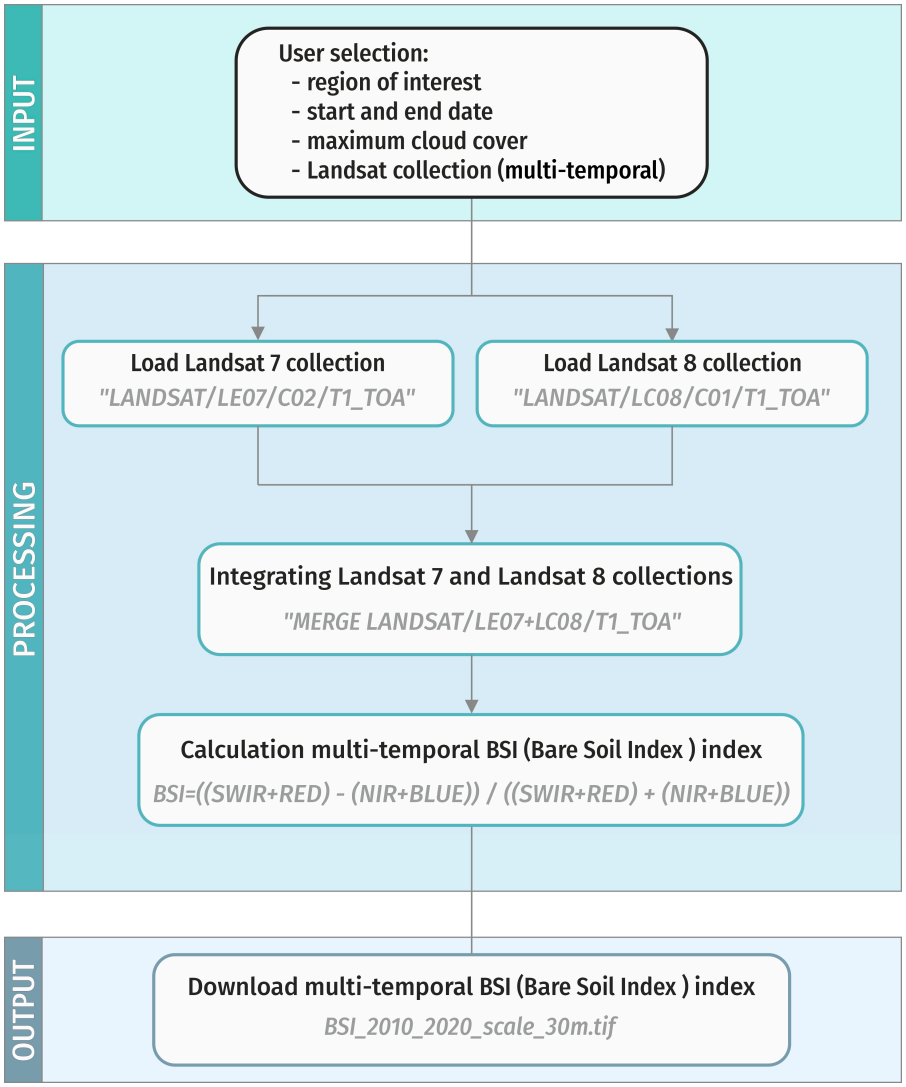

Figure 3. Flowchart of downloading multi-temporal satellite images and the spectral BSI using the GEE platform.

2.4. Application of the Spectral Index (Bare Soil Index—BSI)

In this study, the BSI was used. The BSI was initially introduced by Rikimaru et al. [83] for monitoring forest conditions or canopy density and stands as one of the most significant spectral indices combining blue spectral channels (BLUE), red spectral channels (RED), near-infrared spectral channels (NIR), and shortwave infrared spectral channels (SWIR) to depict the degree of bare soil presence using Equation (3). The RED and SWIR spectral channels reflect the mineral composition of the analyzed soil, while the BLUE and NIR spectral channels represent vegetation presence. With the development of satellites and their sensors and computer technology, there are now various formulas and methods for obtaining spectral indices for bare soil detection [72,84–94]. Based on available Landsat mission satellite imagery, the BSI was derived using Equation (3) [83,95]:

$$\mathrm{BSI} = \frac{(\mathrm{SWIR} + \mathrm{RED}) - (\mathrm{NIR} + \mathrm{BLUE})}{(\mathrm{SWIR} + \mathrm{RED}) + (\mathrm{NIR} + \mathrm{BLUE})} \quad (3)$$

The value of the BSI ranges from −1 to +1, with positive values indicating a greater presence of bare soil and impervious surfaces. In contrast, negative values indicate the presence of vegetation and porous surfaces. Since the BSI is a numerical indicator with values ranging from −1 to +1, the next step involves transforming the spectral index to map erosion processes and assigning values to the coefficient φ, i.e., the numerical equivalent of visible and clearly expressed erosion processes. The transformed BSI is converted into the fractional bare soil cover. Fractional bare soil cover represents the proportion of bare soil within one pixel. The term 'fractional cover' refers to the ratio of vertically projected surfaces (e.g., vegetation, bare soil, and urban areas) to the total surface area [96].

The proportional area of each component in a pixel represents the weighting factor of each component. According to Carlson and Ripley, and Gutman and Ignatov [97,98], the proportional area of bare soil in the fractional cover was obtained based on applying Equation (4) to the fractional vegetation cover [97,98]. In the original formula [97,98], a spectral index for vegetation, i.e., the NDVI, was used, while the spectral index BSI was used to identify bare soil. The obtained values of the fractional bare soil cover range from 0 to 1, where 0 represents areas without bare soil and impervious surfaces, while 1 represents the 100% involvement of bare soil and impervious surfaces. The values of the fractional bare soil cover are the same as those shown in Table 2 and represent the coefficient of the types and extent of erosion and slumps (φ). Based on the observations mentioned above, Equation (4) was applied for the parameter coefficient (φ):

$$\varphi = \frac{BSI - BSI_{min}}{BSI_{max} - BSI_{min}} \quad (4)$$

φ—The coefficient of type and extent of erosion; BSI—the bare soil index; BSImax—a value representing bare soil in the BSI layer; BSImin—a value representing vegetation in the BSI layer.

2.5. The Accuracy Assessment and Validation of the Coefficient φ

The obtained values of the coefficient (φ) based on the application of satellite imagery and its products (the spectral index and fractional cover) were analyzed using accuracy assessment following field investigations. Accuracy assessment is a crucial component and focus of significant studies within the context of accuracy assessment issues [99–102]. The most effective and common way of representing the accuracy of classification data (imagery) obtained through RS is in the form of a confusion matrix or error matrix, based on which accuracy measures are calculated [103–107]. The confusion matrix serves as the basis for obtaining various accuracy measures such as the overall accuracy (OA), user's accuracy (UA), producer's accuracy (PA), and the Kappa statistic [102,104,108–110].

3. Results

3.1. The Collection of Satellite Imagery and Creation of Thematic Maps of the Types and Extent of Erosion and Slumps

After applying Equation (3) in the GEE platform, the thematic map of the spectral BSI was downloaded in a raster format (*.geotiff) at the original resolution of 30 m. The obtained thematic map of the BSI represents the average value of the index that was created based on available satellite products and as such can be used in ArcMap 10.8.2 to apply the transformation of the spectral BSI into the fraction of bare soil cover. Figure 4 illustrates the spatial distribution of the average spectral BSI, one of the most commonly used indices for mapping bare soil and non-porous surfaces. The BSI values in the research area range from −0.58 to +0.26, with a mean value of −0.24 (Figure 5).

By applying Equation (4), a thematic map of the coefficient of the types and extent of erosion and slumps (φ) was obtained. The resulting thematic map, with a spatial resolution of 30 m, is projected in the WGS84/UTM zone 34N and displays values ranging from 0 to 1 (Figure 6). Pixels with values of 0 represent areas without visible traces of erosion processes, while 1 represents areas fully affected by gully and rill processes or deep-type erosion

processes (deepening, incision, and slumps). A histogram distribution of the coefficient φ values is shown in Figure 7. The average value of the coefficient of visible and clearly expressed erosion processes (φ) for the observed period is 0.39, which, according to Table 2, indicates that approximately 35% of the area of the FBiH is affected by surface erosion. In contrast, the remaining part of the area is preserved. The individual categories of the coefficient of the types and extent of erosion and slumps (φ) are shown in Figure 8.

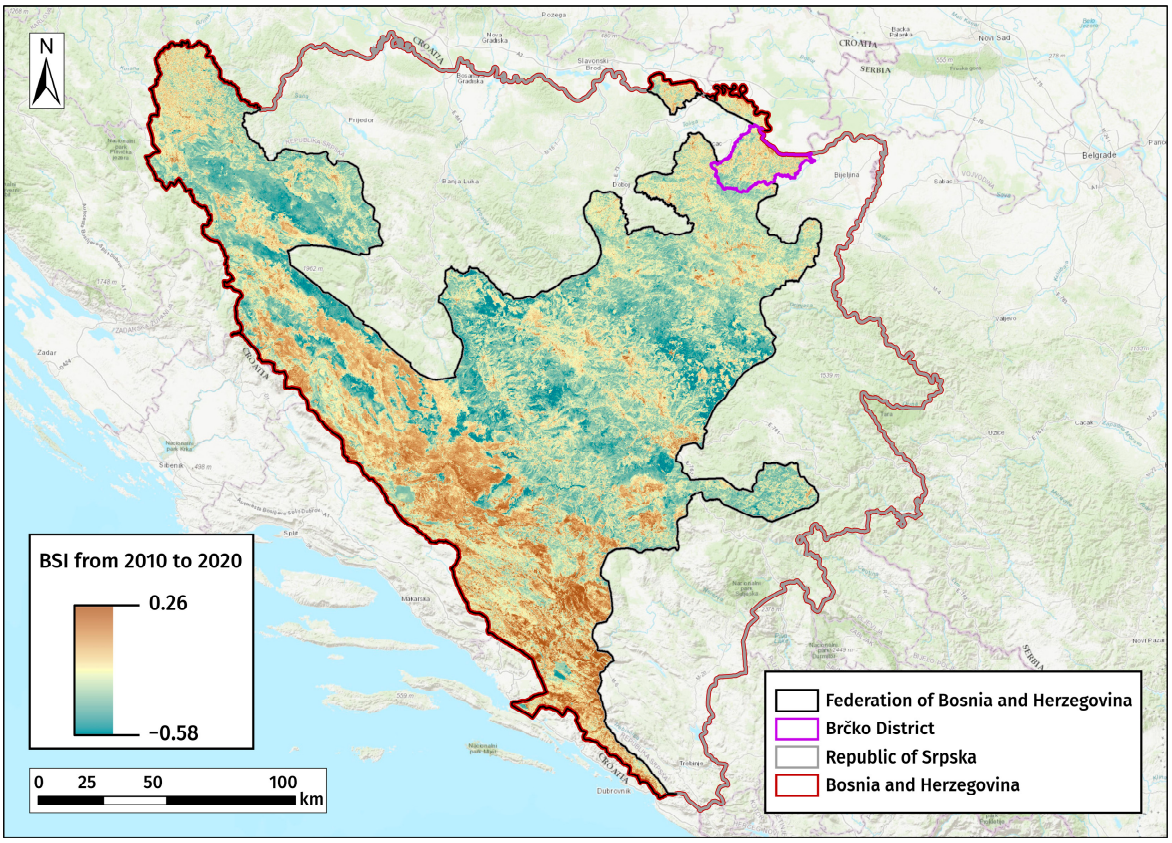

Figure 4. The spatial distribution of the average BSI from 1 January 2010 to 31 December 2020.

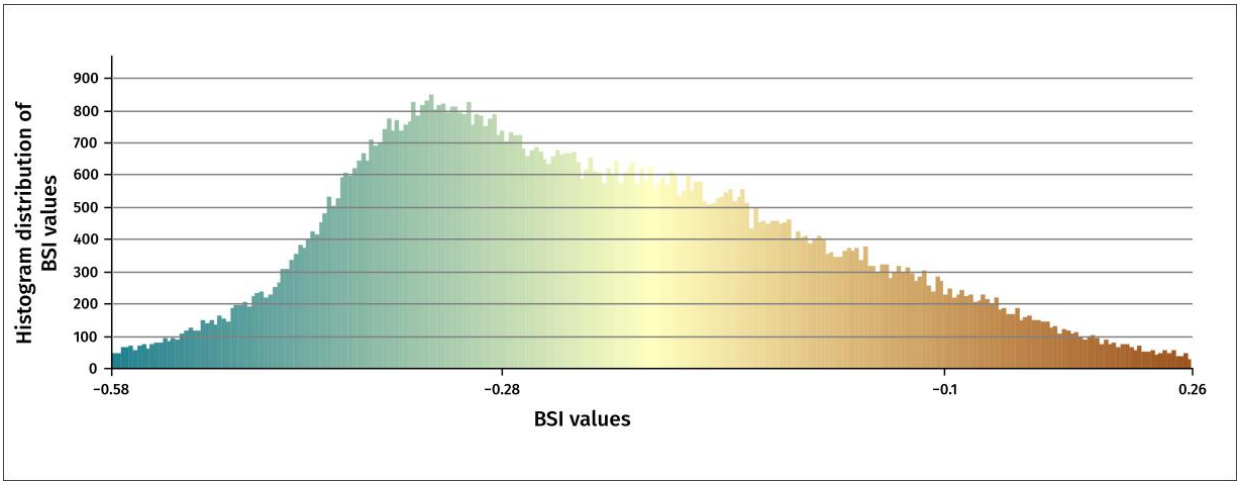

Figure 5. The histogram distribution of the average BSI from 1 January 2010 to 31 December 2020.

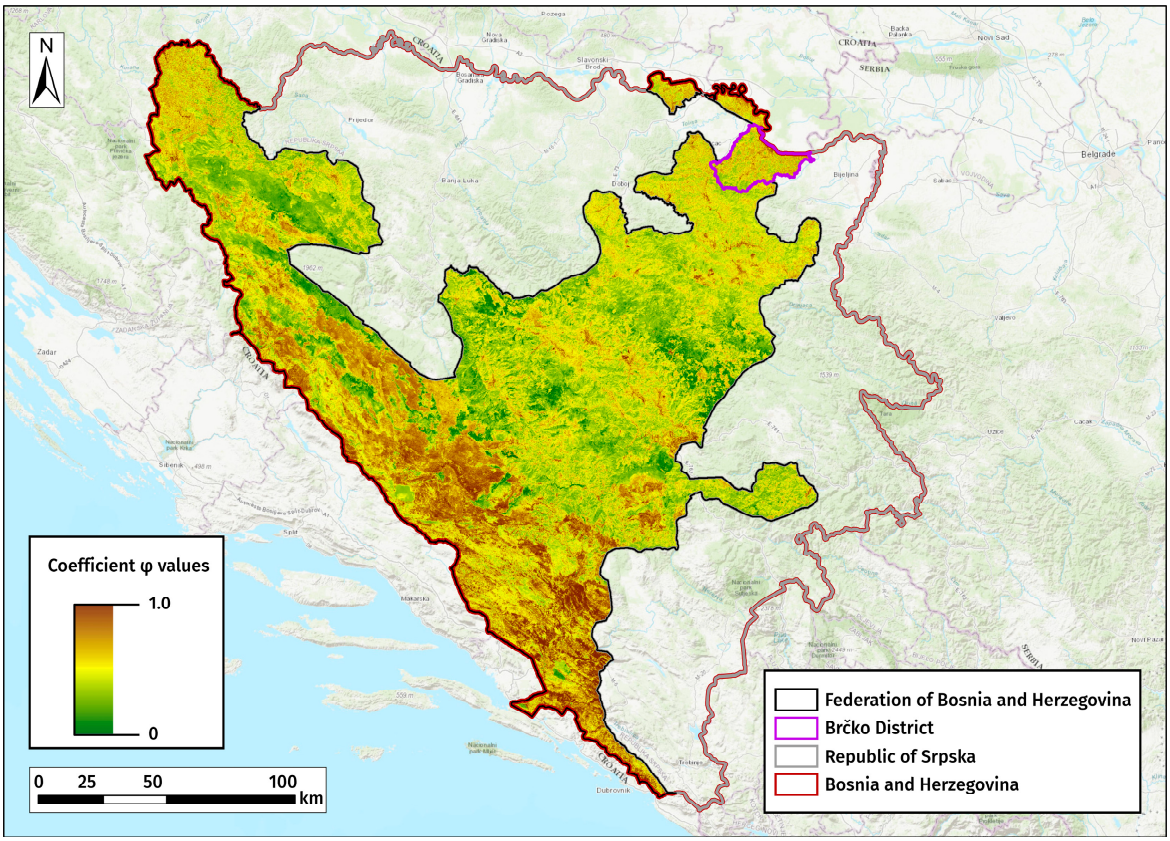

Figure 6. The spatial distribution of the coefficient φ from 1 January 2010 to 31 December 2020.

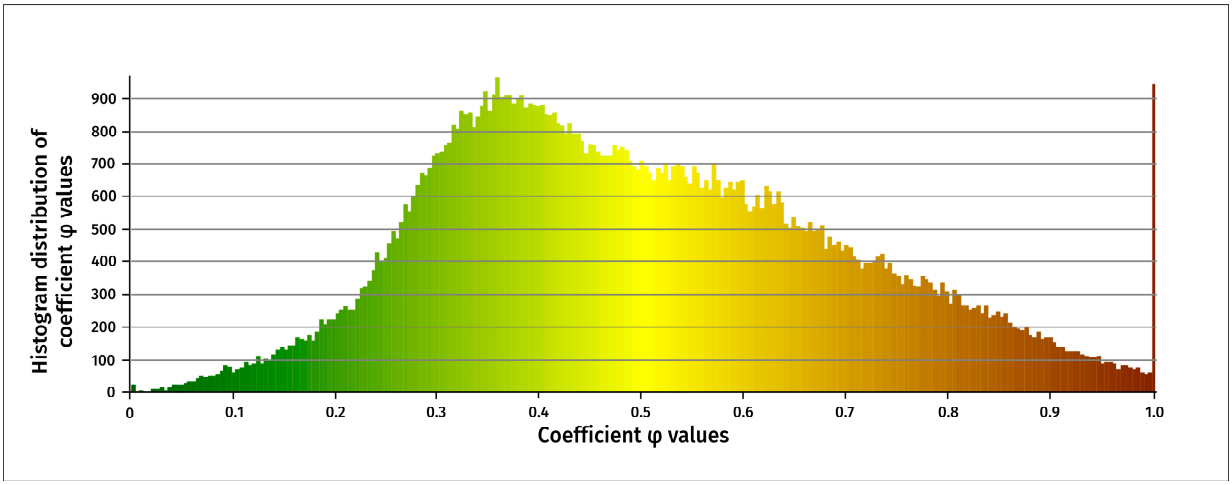

Figure 7. The histogram distribution of the coefficient φ from 1 January 2010 to 31 December 2020.

3.2. Validation of the Obtained Results (Accuracy Assessment)

After conducting the complete procedure of obtaining the coefficient of the types and extent of erosion and slumps (φ) using the spectral BSI, an accuracy assessment was performed to determine the quality of the obtained coefficient φ through RS. The accuracy assessment procedure employed involved comparing samples from the map obtained using the spectral BSI with reference samples (Figure 9). Reference samples for accuracy assessment were collected visually based on field surveys and gathering photo documentation, completing field forms, and using orthophotos and satellite images.

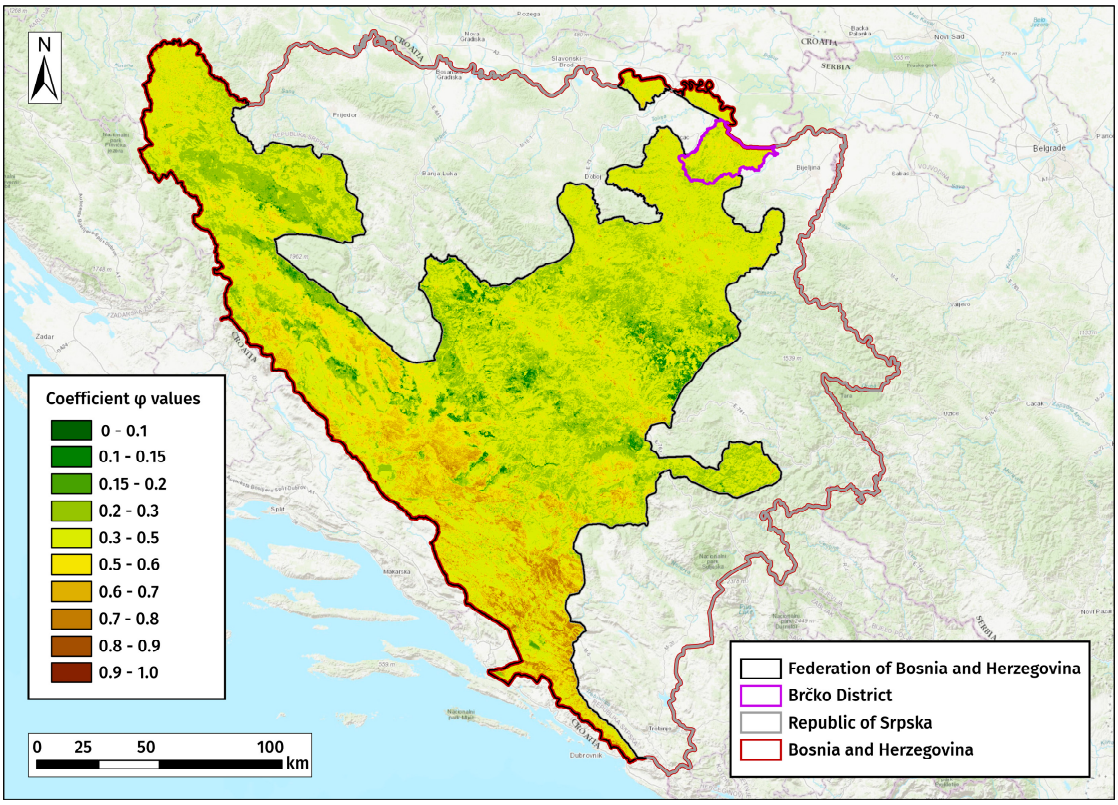

Figure 8. The categories of the coefficient of type and extent of erosion and slumps (φ) from 1 January 2010 to 31 December 2020.

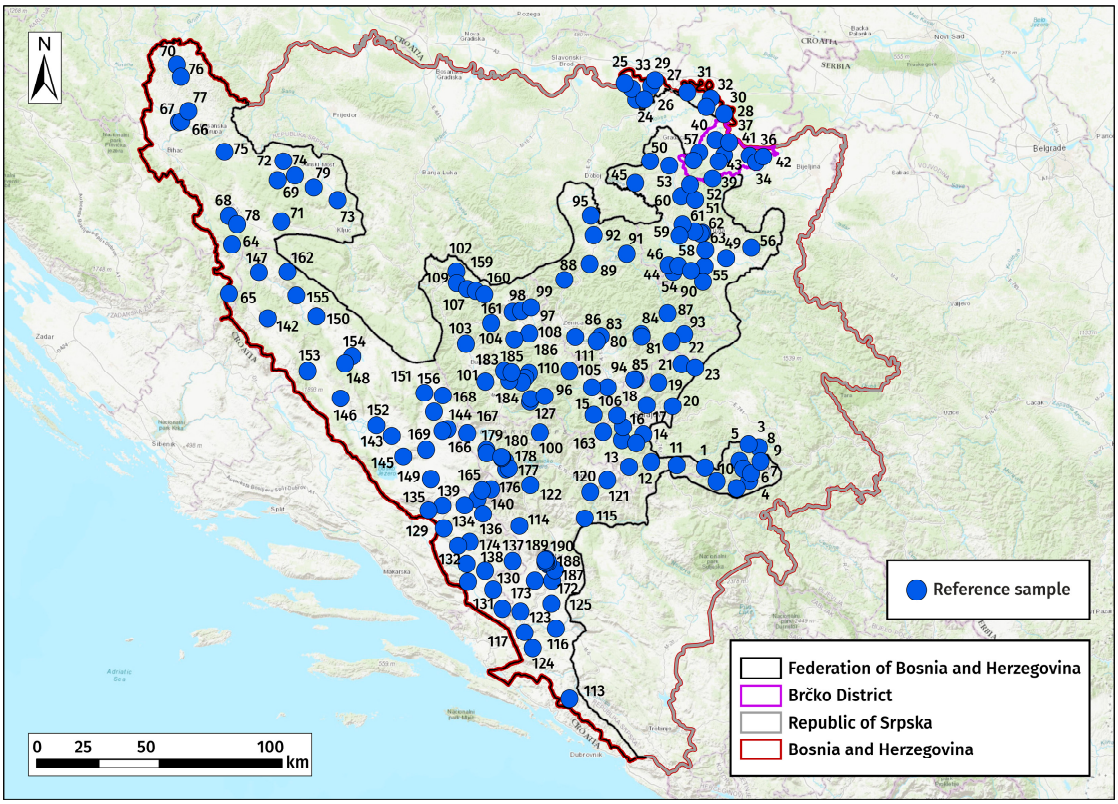

Figure 9. The spatial distribution of reference samples for validating the coefficient φ values.

Table 3 presents basic information about the created reference samples used to validate each category of the φ coefficient values, depending on the conditions in the field. A total of 190 ground reference samples were used, with 8 samples used for φ = 0.1. To assess the accuracy of φ = 0.15, eight samples were used, while only two reference samples available in the field were analyzed for φ = 0.2. A total of 11 samples were validated for φ = 0.3, and 68 samples were analyzed for φ = 0.5 accuracy assessment. For φ = 0.6, 43 samples were analyzed, and 28 samples were assessed for φ = 0.7 during the validation process. A total of 12 samples were employed to check the accuracy assessment for φ = 0.8, while 9 samples were analyzed for φ = 0.9. For φ = 1.0 (areas fully covered by gully erosion and ravine processes, i.e., deep erosion processes), only one sample recorded in the field was analyzed. All these samples were determined based on field surveys conducted in various terrain accessibility and passability conditions, including in the presence of roads, forest paths, and minefields.

Table 3. The total number of reference samples for validating the φ coefficient values.

Value of Coefficient φ	The Number of Samples for Validation.
0.1	8
0.15	8
0.2	2
0.3	11
0.5	68
0.6	43
0.7	28
0.8	12
0.9	9
1.0	1
Total	190

The accuracy assessment method is based on a pixel-level classification accuracy estimation performed using a confusion matrix (error matrix). To compute the confusion matrix and accuracy measures (OA, UA, PA, and Kappa statistics), the R programming language was utilized [111]. Table 4 shows the confusion matrix with accuracy measures for φ values obtained based on the spectral BSI and field investigation work.

Table 4. The confusion matrix with accuracy measures for φ values obtained through field investigations, multispectral satellite imagery, and the BSI.

		Reference Values of the Coefficient φ from the Field											
	Coefficient φ	0.1	0.15	0.2	0.3	0.5	0.6	0.7	0.8	0.9	1.0	Total	UA (%)
Values of the coefficient φ based on remote sensing	0.1	8	0	0	0	0	0	0	0	0	0	8	100
	0.15	0	8	0	0	0	0	0	0	0	0	8	100
	0.2	0	0	1	2	0	0	0	0	0	0	3	33.33
	0.3	0	0	0	8	3	0	0	0	0	0	11	72.73
	0.5	0	0	1	1	60	2	1	0	0	0	65	92.31
	0.6	0	0	0	0	4	37	1	0	0	0	42	88.10
	0.7	0	0	0	0	1	4	19	0	0	0	24	79.17
	0.8	0	0	0	0	0	0	7	12	0	0	19	63.16
	0.9	0	0	0	0	0	0	0	0	9	0	9	100
	1.0	0	0	0	0	0	0	0	0	0	1	1	100
	Total	8	8	2	11	68	43	28	12	9	1	190	OA (%) 85.79
	PA (%)	100	100	50	72.73	88.24	86.05	67.86	100	100	100		Kappa 0.82

Figures 10–12 provide examples of the types and extent of erosion and slumps in the territory of the FBiH and the BD. Erosion processes are depicted based on field investigations, represented as validation samples for accuracy assessment, satellite imagery, and the thematic map of the φ coefficient obtained as the product of RS incorporating the spectral BSI. Data for other representative samples are presented in the Supplementary Materials.

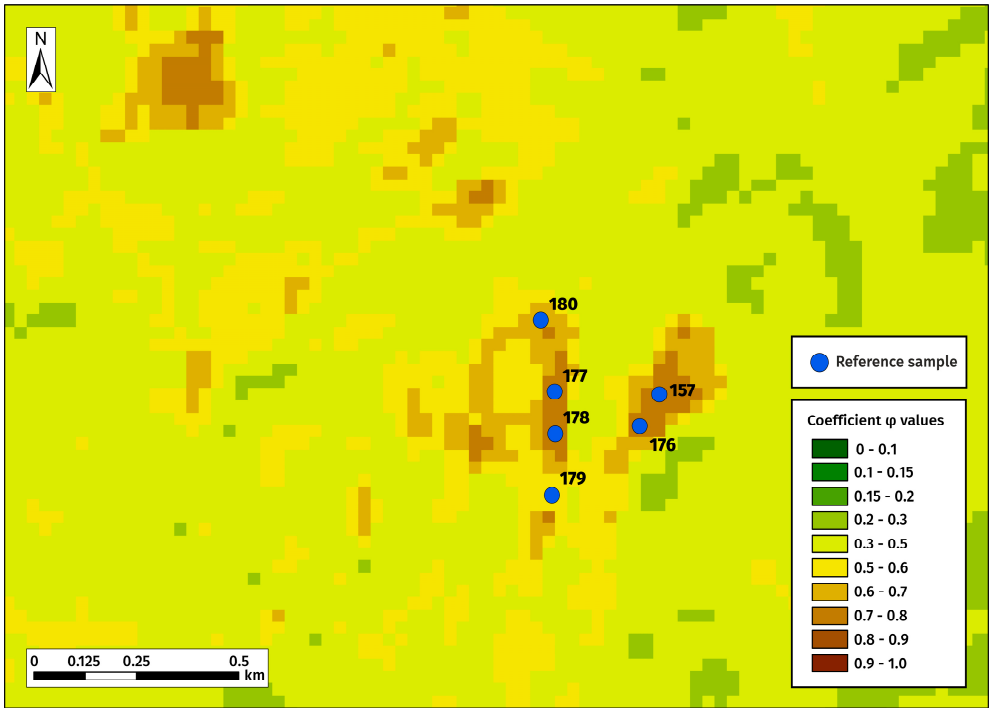

Figure 10. Coefficient φ obtained based on the BSI (sample 157 with φ = 0.81; sample 176 with φ = 0.75; sample 177 with φ = 0.75; sample 178 with φ = 0.78; sample 179 with φ = 0.52; sample 180 with φ = 0.69).

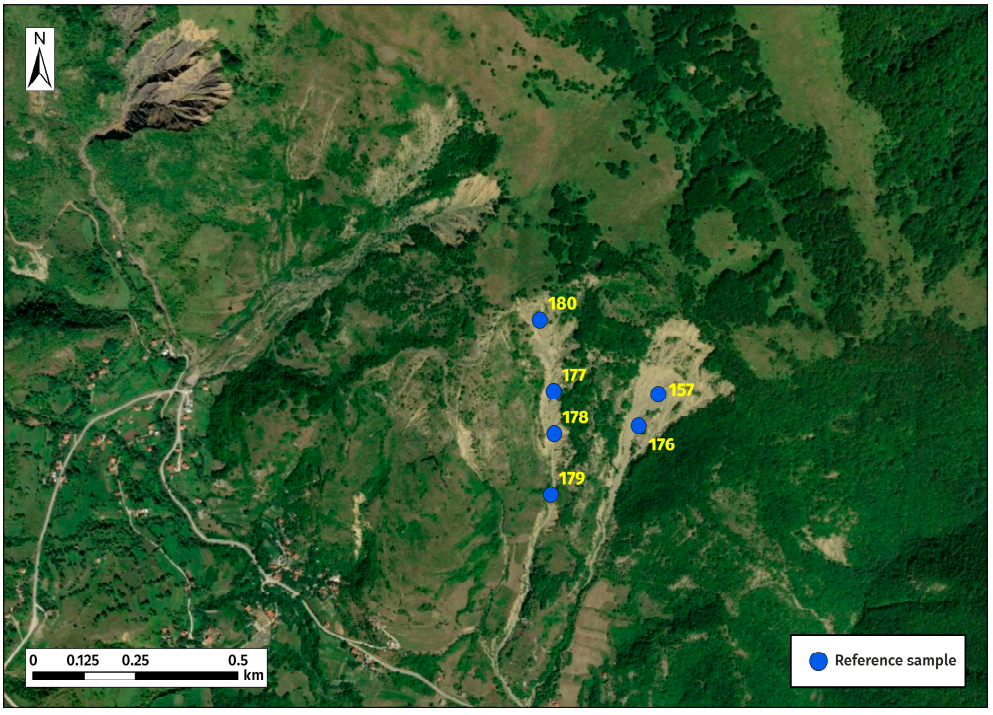

Figure 11. A satellite image with samples 157, 176, 177, 178, 179, and 180.

Figure 12. Samples 157, 176, 177, 178, 179, and 180 after field investigations.

4. Discussion

The application of RS techniques in various scientific, societal, and economic fields has provided the motivational impetus for the development of different types of platforms and sensors with varying spatial and temporal resolutions [103,104]. However, RS data alone cannot directly provide significant information on soil erosion, which might be a reason why RS data have not been widely used for soil erosion assessment or mapping [73]. The development of GIS software and techniques for the collection and transformation of spectral channels has led to advancements in the field of soil erosion assessment and mapping. One of the most widely used methods for soil erosion assessment and mapping is the application of spectral indices, which are primary products of spectral channels. In the context of the BSI which is commonly used to identify areas susceptible to erosion, the constituent variables typically include spectral bands associated with soil reflection in the visible and NIR wavelengths. These bands are sensitive to the amount of bare soil exposed in an area, as bare soil tends to have different spectral characteristics compared to areas covered with vegetation [75,94].

The significance of these constituent variables lies in their ability to distinguish bare soil from vegetated surfaces. Bare soil tends to reflect more light in the visible spectrum and less in the NIR spectrum compared to vegetation. By analyzing the combination of reflectance values in these spectral ranges, the BSI can effectively identify areas exposed to erosion processes.

Moreover, the reliability of this index in quantifying the extent of erosion is supported by empirical validation and calibration against ground truth data. This involves comparing the index results with field observations of erosion severity to assess the accuracy of this index in identifying eroded areas. Additionally, statistical measures such as the OA, UA, PA, and the Kappa statistic are often used to quantify this index's performance in delineating erosion [73,75,84]. In summary, the physical significance of this index's constituent variables lies in their ability to capture the spectral differences between bare soil and vegetated surfaces, while the reliability of this index in quantifying the extent of erosion has been confirmed through empirical validation and statistical analysis.

When dealing with mixed pixels in relation to the BSI, several approaches can be applied to address this challenge effectively. One method involves using the Modified Bare Soil Index (MBSI), which enhances the ability to discriminate between bare soil and urban areas [84,88]. Additionally, combining several spectral indices, such as the Normalized Difference Tillage Index (NDTI) [90,91] and the Dry Bare Soil Index (DBSI) [88], can help improve the accuracy of distinguishing between different soil characteristics, particularly in areas with similar spectral responses, such as bare soil and built-up surfaces [87,93,94]. Moreover, using a multi-index approach that incorporates multiple spectral indices and involves the use of advanced techniques such as cloud computing platforms and machine learning algorithms can significantly enhance the accuracy of identifying and classifying bare soil amidst mixed pixels [84,91,92,95]. This approach has shown promising results, with high accuracy rates and improved performance in distinguishing between built-up areas and barren land, even in challenging environments with complex canopies and mixed soil features. The next advancement presented in this study involves determining the empirical relationship between the spectral BSI and the calculated φ coefficient to map erosion processes of varying intensities and develop a soil erosion map using the EPM.

According to the method developed by Gavrilović, the values of the φ coefficient are categorized into ten classes, which are shown in Table 2 [24]. The original motivation behind this coefficient is related to the percentage of eroded surfaces, which is expressed with a maximum value of 1 (100%) [24]. Nowadays, various methods exist for obtaining φ values, ranging from assigning vector databases on digitized land cover or substrates representing erosion landforms [32,35–37,40,41,43,44,50–53] to using ready-made raster databases on terrain sensitivity, landslide susceptibility maps, and land degradation [33,49,55] and the application of various satellite images in combination with one or more multispectral channels [46–48]. According to the original approach, field investigations are proposed for determining the φ coefficient. This fieldwork involves surveillance, i.e., exploring the terrain with a detailed collection of relevant data on elements indicating the occurrence of specific erosion categories—the types and extent of erosion and slumps, vegetation cover status, land use, etc.—which are then entered into appropriate field forms. Based on this, the φ coefficient represents the only parameter in the EPM with a subjective component, deviating the most from the attributes of an "empirical erosion model". De Vente and Poesen [20] classified this method as a 'semi-quantitative' erosion model.

The structures of field patterns are key elements in creating a soil erosion map as they contains essential elements from previous studies' data collection and analysis results and relevant elements that can only be determined in the field. The data collected from studies include general information about the subject area, such as its position with respect to the administrative area (municipality, canton, etc.) and the watershed and subwatershed. In the study data collection process, essential physical-geographical characteristics of the subject area are determined, as well as elements (parameters) for determining soil erodibility and soil protection. The field data collection process includes obtaining elements for calibrating input parameters, such as the types and extent of erosion processes and slumps, the land cover structure, and land use practices. Field patterns with accompanying photo documentation play a significant role in assessing the accuracy and correcting the input parameters or accuracy assessment results of the φ coefficient to obtain quantitative guidelines for creating a representative soil erosion map.

Representative samples were selected for each category of the φ coefficient value, which had an unbiased representation of the entities the categories depicted. The survey locations were selected based on available satellite and orthophoto imagery and the thematic map of φ coefficient values obtained using the spectral BSI. Data influencing the nature of fieldwork, such as minefield zones, road infrastructure, protected areas, hydrographic networks, populated areas, etc., were also utilized. Based on the given criteria, 190 survey locations were identified for field visits and the determination of field patterns evenly distributed across the territory of the FBiH and BD to achieve a uniform distribution relative to the researched area.

The validation of RS results and the assessment of the accuracy of the derived estimates are crucial but must account for the uncertainty caused by differences in spatial and temporal scales between remote sensor data and reference data used for validation. Validating results obtained from analyses conducted at different scales requires careful consideration of scale-related uncertainties. Various approaches have been developed to address this challenge and verify results across different scales, such as spatial aggregation or disaggregation, sampling design, error propagation, cross-scale validation, model calibration and validation, statistical metrics, uncertainty analysis, and expert judgment [71,72,74,84,90,94,95]. In the context of accuracy assessment and the validation of results, statistical metrics are commonly used, with one of the most widely applied being the confusion matrix or error matrix, which is used to calculate accuracy measures [102,104,107].

The confusion matrix in Table 4 demonstrates uniform accuracy across all categories of the types and extent of erosion, amounting to 85.79%. Upon category-wise analysis of the φ coefficient values, the UA was found to be lowest for φ = 0.2 (33.33%) and φ = 0.8 (63.16%). Significantly higher UA values were observed for φ = 0.5 (92.31%), followed by φ = 0.1 (100%), φ = 0.15 (100%), φ = 0.9 (100%), and φ = 1.0 (100%). The low UA for values of 33.33% and 63.16% are likely due to the mismatch between the predicted and actual classes in these categories. The UA is the probability that a value predicted to be in a certain class really is that class. It is calculated by dividing the number of correctly classified pixels in a class by the total number of pixels predicted to be in that class. In this case, if the predicted classes for values of 33.33% and 63.16% do not match the actual classes, the user accuracy will be low. This could be due to various factors such as incorrect classification, noise or errors in data, insufficient training data or complexity of categories. Regarding the PA, lower values were noted for φ = 0.2 (50%) and φ = 0.7 (67.86%). Higher PA was evident in the values for φ = 0.1 (100%), φ = 0.15 (100%), φ = 0.8 (100%), φ = 0.9 (100%), and φ = 1.0 (100%). The low PA can be attributed to several factors, in addition to those affecting UA, such as insufficient training data, spatial resolution, and temporal factors. To improve the UA and PA for these categories, it may be necessary to refine the classification algorithm, collect more representative training data (especially for categories φ = 0.2, φ = 0.3, φ = 0.7, and φ = 0.8), use additional techniques to handle complex categories effectively, and address any issues with data quality or spatial resolution. Applying Kappa statistics revealed an accuracy of 0.82, indicating a high level of accuracy in the values of the types and extent of erosion and slumps using the spectral BSI. According to the classification proposed by Landis and Koch [109], Kappa statistics show that the classified data satisfactorily align with representative samples [104,108,109]. The obtained raster layer of the φ coefficient can be applied to create soil erosion maps and calculate erosion material production and sediment transport.

5. Conclusions

This research highlights the important role of RS data in mapping soil erosion and erosion processes, and it provides a new approach for identifying the φ coefficient, which is one of the sensitive parameters in the EPM. According to the original method, this coefficient is determined directly in the field through the visual inspection of erosion processes and the delineation of their extent. Given that the field identification of this coefficient is a highly demanding process, the main advantage presented in this study is the application of the spectral BSI and its empirical relationship in mapping erosion processes.

By applying this approach to determine the φ coefficient and using satellite imagery, hidden traces of erosion processes that are sources of erosion material and the cause of flash floods in hilly and mountainous areas can be identified. These hidden traces of erosion processes may not be visible in the field due to the presence of dense vegetation in forests or crops on agricultural land. Thus, by using multispectral satellite images during both vegetative and non-vegetative periods and applying combinations of different spectral bands, it is possible to distinguish erosion traces despite the presence of dense vegetation. The availability of a time series of multispectral satellite images obtained on a monthly

basis is a key element in monitoring the occurrence of various types of erosion processes (surface, mixed, and deep) in the field.

The proposed approach can further be applied in the EPM model to calculate soil loss, sediment transport, and sediment production and to create a soil erosion map. This process increases the efficiency of creating erosion maps, accelerates the process itself, and reduces the number of field visits required, especially for larger study areas, at regional and national levels. Additionally, the developed an erosion map significantly contributes to decision-making, strategy formulation, and planning in the fields of erosion control, the designation of erosion-prone areas, and flood defense planning.

Supplementary Materials: The following supporting information can be downloaded at: https://www.mdpi.com/article/10.3390/rs16132390/s1, Figure S1: Coefficient φ obtained based on the BSI (sample 158 with φ = 0.84; sample 175 with φ = 0.90); Figure S2: Satellite image with samples 158 and 175; Figure S3: Coefficient φ obtained based on the BSI (sample 112 with φ = 0.73; sample 170 with φ = 0.85; sample 187 with φ = 0.42; sample 188 with φ = 0.74; sample 189 with φ = 0.77; sample 190 with φ = 0.82); Figure S4: Satellite image with samples 112, 170, 187, 188, 189, and 190; Figure S5: Samples 112, 170, 187, 188, 189, and 190 after field investigations; Figure S6: Coefficient φ obtained based on the BSI (sample 128 with φ = 0.67); Figure S7: Satellite image with sample 128; Figure S8: Sample 128 after field investigations; Figure S9: Sample 128 after field investigations; Figure S10: Coefficient φ obtained based on the BSI (sample 133 with φ = 0.71); Figure S11: Satellite image with sample 133; Figure S12: Sample 133 after field investigations; Figure S13: Coefficient φ obtained based on the BSI (sample 47 with φ = 0.57); Figure S14: Satellite image with sample 47; Figure S15: Sample 47 after field investigations; Figure S16: Coefficient φ obtained based on the BSI (sample 84 with φ = 0.50); Figure S17: Satellite image with sample 84; Figure S18: Sample 84 after field investigations; Figure S19: Coefficient φ obtained based on the BSI (sample 80 with φ = 0.72); Figure S20: Satellite image with sample 80; Figure S21: Sample 80 after field investigations.

Author Contributions: Conceptualization, S.P. and B.R.; methodology, S.P., B.R. and R.R.; software, S.P.; validation, V.M.; formal analysis, V.M.; writing—original draft preparation, S.P., B.R. and R.R.; writing—review and editing, S.P., B.R. and R.R.; visualization, S.P. and B.R. All authors have read and agreed to the published version of the manuscript.

Funding: This research was funded by (1). Europeaid/140327/DH/SER/BA—Technical Assistance for Preparation of Erosion Protection Plans and Technical Design Documentation for Flood Protecting Infrastructure for Selected Priority Areas in Bosnia and Herzegovina and (2). The Ministry of Education, Science and Technological Development, which finances the scientific research of the University of Belgrade, the Faculty of Forestry on the basis of an agreement of the following realization number: 451-03-65/2024-03/200169.

Data Availability Statement: Data are contained within the article.

Conflicts of Interest: The authors declare no conflicts of interest.

References

1. Borrelli, P.; Robinson, D.A.; Panagos, P.; Lugato, E.; Yang, J.E.; Alewell, C.; Wuepper, D.; Montanarella, L.; Ballabio, C. Land Use and Climate Change Impacts on Global Soil Erosion by Water (2015–2070). *Proc. Natl. Acad. Sci. USA* **2020**, *117*, 21994–22001. [CrossRef] [PubMed]
2. Ouyang, D.; Bartholic, J. Predicting Sediment Delivery Ratio in Saginaw Bay Watershed. In Proceedings of the 22nd National Association of Environmental Professionals Conference, Orlando, FL, USA, 19–23 May 1997; pp. 659–671.
3. Noori, H.; Siadatmousavi, S.M.; Mojaradi, B. Assessment of Sediment Yield Using RS and GIS at Two Sub-Basins of Dez Watershed, Iran. *Int. Soil Water Conserv. Res.* **2016**, *4*, 199–206. [CrossRef]
4. De Koning, G.H.J.; Veldkamp, A.; Fresco, L.O. Land Use in Ecuador: A Statistical Analysis at Different Aggregation Levels. *Agric. Ecosyst. Environ.* **1998**, *70*, 231–247. [CrossRef]
5. Le Bissonnais, Y.; Montier, C.; Jamagne, M.; Daroussin, J.; King, D. Mapping Erosion Risk for Cultivated Soil in France. *Catena* **2002**, *46*, 207–220. [CrossRef]
6. Martínez-Casasnovas, J.A. A Spatial Information Technology Approach for the Mapping and Quantification of Gully Erosion. *Catena* **2003**, *50*, 293–308. [CrossRef]
7. Pandey, A.; Chowdary, V.M.; Mal, B.C. Identification of Critical Erosion Prone Areas in the Small Agricultural Watershed Using USLE, GIS and Remote Sensing. *Water Resour. Manag.* **2007**, *21*, 729–746. [CrossRef]

8. Jain, M.K.; Das, D. Estimation of Sediment Yield and Areas of Soil Erosion and Deposition for Watershed Prioritization Using GIS and Remote Sensing. *Water Resour. Manag.* **2010**, *24*, 2091–2112. [CrossRef]
9. Veldkamp, A.; Fresco, L.O. CLUE: A Conceptual Model to Study the Conversion of Land Use and Its Effects. *Ecol. Modell.* **1996**, *85*, 253–270. [CrossRef]
10. Estrany, J.; Garcia, C.; Walling, D.E. An Investigation of Soil Erosion and Redistribution in a Mediterranean Lowland Agricultural Catchment Using Caesium-137. *Int. J. Sediment Res.* **2010**, *25*, 1–16. [CrossRef]
11. van Lynden, G.W.J. *European Soil Resources: Current Status of Soil Degradation, Causes, Impacts and Need for Action*; Council of Europe Press: Luxembourg, 1995; 99p.
12. European Commission Soil Thematic Strategy, COM(2006) 231—European Environment Agency. Available online: https://www.eea.europa.eu/policy-documents/soil-thematic-strategy-com-2006-231 (accessed on 19 March 2024).
13. Panagos, P.; Christos, K.; Cristiano, B.; Ioannis, G. Seasonal Monitoring of Soil Erosion at Regional Scale: An Application of the G2 Model in Crete Focusing on Agricultural Land Uses. *Int. J. Appl. Earth Obs. Geoinf.* **2014**, *27*, 147–155. [CrossRef]
14. Panagos, P.; Borrelli, P.; Poesen, J.; Ballabio, C.; Lugato, E.; Meusburger, K.; Montanarella, L.; Alewell, C. The New Assessment of Soil Loss by Water Erosion in Europe. *Environ. Sci. Policy* **2015**, *54*, 438–447. [CrossRef]
15. López-Vicente, M.; Navas, A.; Gaspar, L.; Machín, J. Advanced Modelling of Runoff and Soil Redistribution for Agricultural Systems: The SERT Model. *Agric. Water Manag.* **2013**, *125*, 1–12. [CrossRef]
16. Eniyew, S.; Teshome, M.; Sisay, E.; Bezabih, T. Integrating RUSLE Model with Remote Sensing and GIS for Evaluation Soil Erosion in Telkwonz Watershed, Northwestern Ethiopia. *Remote Sens. Appl. Soc. Environ.* **2021**, *24*, 100623. [CrossRef]
17. Duarte, L.; Cunha, M.; Teodoro, A.C. Comparing Hydric Erosion Soil Loss Models in Rainy Mountainous and Dry Flat Regions in Portugal. *Land* **2021**, *10*, 554. [CrossRef]
18. Russell, S.; Harmon, W.W.D. (Eds.) *Landscape Erosion and Evolution Modeling*; Springer: New York, NY, USA, 2001. [CrossRef]
19. Morgan, R.P.C.; Quinton, J.N. Erosion Modeling. In *Landscape Erosion and Evolution Modeling*; Springer: New York, NY, USA, 2001; pp. 117–143. [CrossRef]
20. de Vente, J.; Poesen, J. Predicting Soil Erosion and Sediment Yield at the Basin Scale: Scale Issues and Semi-Quantitative Models. *Earth-Sci. Rev.* **2005**, *71*, 95–125. [CrossRef]
21. de Vente, J. Soil Erosion and Sediment Yield in Mediterranean Geoecosystems—Scale Issues, Modelling and Understanding. Ph.D. Thesis, Katholieke Universiteit, Leuven, Belgium, 2009.
22. Hajigholizadeh, M.; Melesse, A.M.; Fuentes, H.R. Erosion and Sediment Transport Modelling in Shallow Waters: A Review on Approaches, Models and Applications. *Int. J. Environ. Res. Public Health* **2018**, *15*, 518. [CrossRef]
23. Renard, K.; Foster, G.; Weesies, G.; McCool, D.; Yoder, D. *Predicting Soil Erosion by Water: A Guide to Conservation Planning with the Revised Universal Soil Loss Equation (RUSLE)*; US Department of Agriculture, Agricultural Research Service: Washington, DC, USA, 1997; No. 703; pp. 65–100.
24. Gavrilović, S. Engineering of Torrents and Erosion. *J. Constr.* **1972**, *292*. (In Serbian)
25. Kostadinov, S. *Bujični Tokovi i Erozija*; Univerzitet u Beogradu, Šumarski Fakultet: Belgrade, Serbia, 2008. (In Serbian)
26. Vučićević, D. *Uređenje Bujičnih Tokova-Priručnik Za Bujičare*; Društvo Bujičara Jugoslavije: Belgrade, Serbia, 1995. (In Serbian)
27. Gavrilović, S. A Method for Estimating the Average Annual Quantity of Sedimentsaccording to the Potency of Erosion. *Bull. Fac. For.* **1962**, *26*, 151–168.
28. Lazarević, R. *Erozija u Bosni i Hercegovini*; Želnid: Belgrade, Serbia, 2010; ISBN 978-86-7307-216-6. (In Serbian)
29. Mincev, I. Development of methodology for determination of protection zones around water reservoirs from aspect of soil erosion and sediment transport. Ph.D. Thesis, Ss. Cyril and Methodius University, Skopje, North Macedonia, 2014.
30. Blinkov, I. Review and Comparison of Water Erosion Intensity in the Western Balkan and EU Countries. *Contributions. Sect. Nat. Math. Biotech. Sci.* **2015**, *36*, 27–42. [CrossRef]
31. Spalević, V.; Ćurović, M.; Billi, P.; Fazzini, M.; Frankl, A.; Nyssen, J. Soil Erosion in the Zim Potok Watershed Polimlje River Basin, Montenegro. In *Proceedings of the Agrosym 2014: Book of Proceedings: Fifth International Scientific Agricultural Symposium "Agrosym 2014", Jahorina, Bosnia and Herzegovina, 23–26 October 2014*; CABI: Wallingford, UK, 2014.
32. Petras, J.; Kuspilic, N.; Kunstek, D. Some Experience on the Prediction of Suspended Sediment Concentrations and Fluxes in Croatia. In Proceedings of the Symposium SI, Seventh IAHS Scientific Assembly, Foz do Igacu, Brazil, 3–9 April 2005; IAHS: Wallingford, UK; 2005; Volume 292, pp. 179–184.
33. Dragičević, N.; Karleuša, B.; Ožanić, N. A Review of the Gavrilović Method (Erosion Potential Method) Application. *Građevinar* **2016**, *68*, 715–725. [CrossRef]
34. Zemljic, M. Calculation of Sediment Load. Evaluation of Vegetation as Anti-Erosive Factor. In *Proceedings of the International Symposium Interpraevent, Villach, Australia*; INTERPRAEVENT: Vienna, Austria, 1971; pp. 379–391.
35. Globevnik, L.; Holjević, D.; Petkovšek, G.; Rubinić, J. *Applicability of the Gavrillović Method in Erosion Calculation Using Spatial Data Manipulation Techniques*; IAHS-AISH Publication: Wallingford, UK, 2003; pp. 224–233.
36. Zorn, M.; Komac, B.; Gabrovec, M. Influence of Land Use Changes on Erosion in the Slovenian Alps. In Proceedings of the Man in the Landscape across Frontiers—IGU-LUCC Central Europe Conference 2007, Slovenia, Austria, Slovakia, Czechia, 28 August–4 September 2007.
37. De Cesare, G.; Beyer Portner, N.; Boillat, J.; Scleiss, A. *Modelling of Erosion and Sedimentation Based on Field Investigation in Alpine Reservoirs of Hydropower Schemes*; Parallel Session 34; German Coastal Engineering Research Council: Hamburg, Germany, 1998.

38. de Vente, J.; Poesen, J.; Bazzoffi, P.; Van Rompaey, A.; Verstraeten, G. Predicting Catchment Sediment Yield in Mediterranean Environments: The Importance of Sediment Sources and Connectivity in Italian Drainage Basins. *Earth Surf. Process. Landf.* **2006**, *31*, 1017–1034. [CrossRef]
39. Fanetti, D.; Vezzoli, L. Sediment Input and Evolution of Lacustrine Deltas: The Breggia and Greggio Rivers Case Study (Lake Como, Italy). *Quat. Int.* **2007**, *173–174*, 113–124. [CrossRef]
40. Milanesi, L.; Pilotti, M.; Clerici, A. The Application of the Erosion Potential Method to Alpine Areas: Methodological Improvements and Test Case. In *Engineering Geology for Society and Territory–Volume 3: River Basins, Reservoir Sedimentation and Water Resources*; Springer: Cham, Switzerland, 2015; pp. 347–350. [CrossRef]
41. Rafaelli, S.; Peviani, M.; Perez Ayala, F. Study of Sediment Yield on the Mountain Cuence Del Rio Iruya (Argentina). In *Proceedings of the IARH AMH, Hydraulic XVIII Latin American Conference, Oaxaca, Mexico*; Springer: Berlin/Heidelberg, Germany; 1998.
42. Stefanidis, P.; Myronidis, D.; Sapountzis, M.; Stathis, D. The Torrent "Sklitrho" in Florina. In *Torrential Environment and Torrent Control System*; Scientific Annals; Department of Forestry and Natural Environment, Aristotelian University of Thessaloniki: Thessaloniki, Greece, 1998; Volume 41, p. 1275.
43. Emmanouloudis, D.; Filippidis, E. A Quantitative Estimation Model of Mountainous Watershed Degradation. In Proceedings of the Kick-Off Workshop on IAHS, Decade of Prediction in Ungauged Basins (PUB), Brasilia, Brazil, 20–22 November 2002.
44. Emmanouloudis, D.A.; Christou, O.P.; Filippidis, E.I. *Quantitative Estimation of Degradation in the Aliakmon River Basin Using GIS*; IAHS-AISH Publication: Wallingford, UK, 2003; pp. 234–240.
45. Kalinderis, I.; Tziaftani, F.; Sapountzis, M.; Kourakli, P.; Stefanidis, P.; Stathis, D. The Risk of Sedimentation of Artificial Lakes, Following the Soil Loss and Degradation Process in the Wider Drainage Basin. Artificial Lake of Smokovo Case Study (Central Greece). In Proceedings of the International Conference LAND CONSERVATION 0905 "Global Change-Challenges for Soil Management from Degradation through Soil and Water Conservation to Sustainable Soil Management, Tara Mountain, Serbia, 26–30 May 2009; refwid:76018.
46. Cherif, K.; Yahia, N.; Bilal, B.; Bilal, B. Erosion Potential Model-Based ANN-MLP for the Spatiotemporal Modeling of Soil Erosion in Wadi Saida Watershed. *Model. Earth Syst. Environ.* **2023**, *9*, 3095–3117. [CrossRef]
47. Ahmed, A.; Adil, D.; Hasna, B.; Elbachir, A.; Lazaar, R. Using EPM Model and GIS for Estimation of Soil Erosion in Souss Basin, Morocco. *Turkish J. Agric.—Food Sci. Technol.* **2019**, *7*, 1228–1232. [CrossRef]
48. Elbadaoui, K.; Mansour, S.; Ikirri, M.; Abdelrahman, K.; Abu-Alam, T.; Abioui, M. Integrating Erosion Potential Model (EPM) and PAP/RAC Guidelines for Water Erosion Mapping and Detection of Vulnerable Areas in the Toudgha River Watershed of the Central High Atlas, Morocco OSEAN-Outermost Regions Sustainable Ecosystem for Entrepreneursh. *Land* **2023**, *12*, 837. [CrossRef]
49. Ali, S.; Al-Umary, F.A.; Salar, S.G.; Al-Ansari, N.; Knutsson, S. GIS Based Soil Erosion Estimation Using EPM Method, Garmiyan Area, Kurdistan Region, Iraq. *J. Civ. Eng. Archit.* **2016**, *10*, 291–308. [CrossRef]
50. Amini, H.; Honarjoo, N.; Jalaliyan, A.; Khalilizadeh, M.; Baharlouie, J. A Comparison of EPM and WEPP Models for Estimating Soil Erosion of Marmeh Watershed in the South Iran. *Agric. For.* **2014**, *60*, 299–315.
51. da Silva, R.M.; Santos, C.A.G.; Silva, A.M. Predicting Soil Erosion and Sediment Yield in the Tapacurá Catchment. *J. Urban Environ. Eng.* **2014**, *8*, 75–82. [CrossRef]
52. Lense, G.H.E.; Parreiras, T.C.; Moreira, R.S.; Avanzi, J.C.; Mincato, R.L. Estimates of Soil Losses by the Erosion Potential Method in Tropical Latosols. *Cienc. Agrotecnologia* **2019**, *43*, e012719. [CrossRef]
53. Kazimierski, L.D.; Irigoyen, M.; Re, M.; Menendez, A.N.; Spalletti, P.; Brea, J.D. Impact of Climate Change on Sediment Yield from the Upper Plata Basin. *Int. J. River Basin Manag.* **2013**, *11*, 411–421. [CrossRef]
54. Otoniel, N.P. *Identificación de Correlaciones Entre La Arga de Lavado y Algunos Parámetros Geomorfológicos y de Uso de Suelo En La Cuenca Del Río Cauca*; Universidad Nacional de Colombia: Bogotá, Colombia, 2015.
55. Bezak, N.; Borrelli, P.; Mikoš, M.; Jemec Auflič, M.; Panagos, P. Towards Multi-Model Soil Erosion Modelling: An Evaluation of the Erosion Potential Method (EPM) for Global Soil Erosion Assessments. *Catena* **2024**, *234*, 107596. [CrossRef]
56. Gavrilović, S. *Torrents in Serbia*; Republic Water Fund and Faculty of Forestry: Belgrade, Serbia, 1975. (In Serbian)
57. Vrieling, A. Satellite Remote Sensing for Water Erosion Assessment: A Review. *Catena* **2006**, *65*, 2–18. [CrossRef]
58. Đomlija, P.; Gazibara, S.B.; Arbanas, Ž.; Arbanas, S.M. Identification and Mapping of Soil Erosion Processes Using the Visual Interpretation of Lidar Imagery. *ISPRS Int. J. Geo-Inf.* **2019**, *8*, 438. [CrossRef]
59. Deligiannakis, G.; Pallikarakis, A.; Papanikolaou, I.; Alexiou, S.; Reicherter, K. Detecting and Monitoring Early Post-Fire Sliding Phenomena Using Uav–Sfm Photogrammetry and t-Lidar-Derived Point Clouds. *Fire* **2021**, *4*, 87. [CrossRef]
60. Alexiou, S.; Deligiannakis, G.; Pallikarakis, A.; Papanikolaou, I.; Psomiadis, E.; Reicherter, K. Comparing High Accuracy T-Lidar and Uav-Sfm Derived Point Clouds for Geomorphological Change Detection. *ISPRS Int. J. Geo-Inf.* **2021**, *10*, 367. [CrossRef]
61. Alexiou, S.; Papanikolaou, I.; Schneiderwind, S.; Kehrle, V.; Reicherter, K. Monitoring and Quantifying Soil Erosion and Sedimentation Rates in Centimeter Accuracy Using UAV-Photogrammetry, GNSS, and t-LiDAR in a Post-Fire Setting. *Remote Sens.* **2024**, *16*, 802. [CrossRef]
62. Kirchhof, W.; Haberäcker, P.; Krauth, E.; Kritikos, G.; Winter, R. Evaluation of LANDSAT Image Data for Land-Use Mapping. *Acta Astronaut.* **1980**, *7*, 243–253. [CrossRef]
63. Newman, M.E.; McLaren, K.P.; Wilson, B.S. Comparing the Effects of Classification Techniques on Landscape-Level Assessments: Pixel-Based versus Object-Based Classification. *Int. J. Remote Sens.* **2011**, *32*, 4055–4073. [CrossRef]

64. Fisher, P.F.; Pathirana, S. The Evaluation of Fuzzy Membership of Land Cover Classes in the Suburban Zone. *Remote Sens. Environ.* **1990**, *34*, 121–132. [CrossRef]
65. Singh, D.; Herlin, I.; Berroir, J.P.; Silva, E.F.; Meirelles, M.S. An Approach to Correlate NDVI with Soil Colour for Erosion Process Using NOAA/AVHRR Data. *Adv. Sp. Res.* **2004**, *33*, 328–332. [CrossRef]
66. Ma, L.; Li, M.; Ma, X.; Cheng, L.; Du, P.; Liu, Y. A Review of Supervised Object-Based Land-Cover Image Classification. *ISPRS J. Photogramm. Remote Sens.* **2017**, *130*, 277–293. [CrossRef]
67. Dorren, L.K.A.; Maier, B.; Seijmonsbergen, A.C. Improved Landsat-Based Forest Mapping in Steep Mountainous Terrain Using Object-Based Classification. *For. Ecol. Manage.* **2003**, *183*, 31–46. [CrossRef]
68. Phiri, D.; Morgenroth, J. Developments in Landsat Land Cover Classification Methods: A Review. *Remote Sens.* **2017**, *9*, 967. [CrossRef]
69. Moskal, L.M.; Styers, D.M.; Halabisky, M. Remote Sensing Monitoring Urban Tree Cover Using Object-Based Image Analysis and Public Domain Remotely Sensed Data. *Remote Sens.* **2011**, *3*, 2243. [CrossRef]
70. Shruthi, R.B.V.; Kerle, N.; Jetten, V.; Abdellah, L.; Machmach, I. Quantifying Temporal Changes in Gully Erosion Areas with Object Oriented Analysis. *Catena* **2015**, *128*, 262–277. [CrossRef]
71. Rahmati, O.; Tahmasebipour, N.; Haghizadeh, A.; Pourghasemi, H.R.; Feizizadeh, B. Evaluating the Influence of Geo-Environmental Factors on Gully Erosion in a Semi-Arid Region of Iran: An Integrated Framework. *Sci. Total Environ.* **2017**, *579*, 913–927. [CrossRef]
72. Garosi, Y.; Sheklabadi, M.; Pourghasemi, H.R.; Besalatpour, A.A.; Conoscenti, C.; Van Oost, K. Comparison of Differences in Resolution and Sources of Controlling Factors for Gully Erosion Susceptibility Mapping. *Geoderma* **2018**, *330*, 65–78. [CrossRef]
73. Cheng, Z.; Lu, D.; Li, G.; Huang, J.; Sinha, N.; Zhi, J.; Li, S. A Random Forest-Based Approach to Map Soil Erosion Risk Distribution in Hickory Plantations in Western Zhejiang Province, China. *Remote Sens.* **2018**, *10*, 1899. [CrossRef]
74. Bammou, Y.; Benzougagh, B.; Abdessalam, O.; Brahim, I.; Kader, S.; Spalevic, V.; Sestras, P.; Ercişli, S. Machine Learning Models for Gully Erosion Susceptibility Assessment in the Tensift Catchment, Haouz Plain, Morocco for Sustainable Development. *J. Afr. Earth Sci.* **2024**, *213*, 105229. [CrossRef]
75. Xu, H.; Hu, X.; Guan, H.; Zhang, B.; Wang, M.; Chen, S.; Chen, M. A Remote Sensing Based Method to Detect Soil Erosion in Forests. *Remote Sens.* **2019**, *11*, 513. [CrossRef]
76. Ristić, R.; Solomun, M.K.; Malušević, I.; Ždrale, S.; Radić, B.; Polovina, S.; Milćanović, V. Healthy Soils—Healthy People: Soil and Human Health—The Reality of the Balkan Region. In *The Soil-Human Health-Nexus*, 1st ed.; CRC Press: Boca Raton, FL, USA, 2020; pp. 223–248. [CrossRef]
77. UNEP. *United Nations Environmental Programme Sarajevo Action Program for Combat Land Degradation and Mitigate the Effects of Drought in Bosnia and Herzegovina*; GEF: Sarajevo, Bosnia and Herzegovina, 2017.
78. CORINE. Land Cover—Copernicus Land Monitoring Service. Available online: https://land.copernicus.eu/en/products/corine-land-cover (accessed on 19 March 2024).
79. Law, M.; Collins, A. *Getting to Know ArcGIS Desktop 10.8*; Esri Press: Redlands, CA, USA, 2021; ISBN 9781589485785.
80. Gorelick, N.; Hancher, M.; Dixon, M.; Ilyushchenko, S.; Thau, D.; Moore, R. Google Earth Engine: Planetary-Scale Geospatial Analysis for Everyone. *Remote Sens. Environ.* **2017**, *202*, 18–27. [CrossRef]
81. Kumar, L.; Mutanga, O. Google Earth Engine Applications Since Inception: Usage, Trends, and Potential. *Remote Sens.* **2018**, *10*, 1509. [CrossRef]
82. GEE. Google Earth Engine Data Catalog. Available online: https://developers.google.com/earth-engine/datasets/catalog/landsat (accessed on 24 May 2024).
83. Rikimaru, A.; Roy, P.; Miyatake, S. Tropical Forest Cover Density Mapping. *Trop. Ecol.* **2002**, *43*, 39–47.
84. Nguyen, C.T.; Chidthaisong, A.; Diem, P.K.; Huo, L.Z. A Modified Bare Soil Index to Identify Bare Land Features during Agricultural Fallow-Period in Southeast Asia Using Landsat 8. *Land* **2021**, *10*, 231. [CrossRef]
85. Rogers, A.S.; Kearney, M.S. Reducing Signature Variability in Unmixing Coastal Marsh Thematic Mapper Scenes Using Spectral Indices. *Int. J. Remote Sens.* **2004**, *25*, 2317–2335. [CrossRef]
86. Azizi, Z.; Najafi, A.; Sohrabi, H. Forest Canopy Density Estimating, Using Satellite Images. *Int. Arch. Photogramm. Remote Sens. Spat. Inf. Sci.—ISPRS Arch.* **2008**, *27*, 1127–1130. [CrossRef]
87. Piyoosh, A.K.; Ghosh, S.K. Development of a Modified Bare Soil and Urban Index for Landsat 8 Satellite Data. *Geocarto Int.* **2018**, *33*, 423–442. [CrossRef]
88. Rasul, A.; Balzter, H.; Ibrahim, G.R.F.; Hameed, H.M.; Wheeler, J.; Adamu, B.; Ibrahim, S.; Najmaddin, P.M. Applying Built-up and Bare-Soil Indices from Landsat 8 to Cities in Dry Climates. *Land* **2018**, *7*, 81. [CrossRef]
89. Deng, Y.; Wu, C.; Li, M.; Chen, R. RNDSI: A Ratio Normalized Difference Soil Index for Remote Sensing of Urban/Suburban Environments. *Int. J. Appl. Earth Obs. Geoinf.* **2015**, *39*, 40–48. [CrossRef]
90. Quemada, M.; Daughtry, C.S.T. Spectral Indices to Improve Crop Residue Cover Estimation under Varying Moisture Conditions. *Remote Sens.* **2016**, *8*, 660. [CrossRef]
91. Sonmez, N.K.; Slater, B. Measuring Intensity of Tillage and Plant Residue Cover Using Remote Sensing. *Eur. J. Remote Sens.* **2016**, *49*, 121–135. [CrossRef]
92. Samira, D.; Souiher, N.; Djamal, B. Extraction of Urban Areas Using Spectral Indices Combination and Google Earth Engine in Algerian Highlands (Case Study: Cities of Djelfa, Messaad, Ain Oussera). *Anu. do Inst. Geocienc.* **2022**, *45*, 44537. [CrossRef]

93. Wentzel, K. Determination of the Overall Soil Erosion Potential in the Nsikazi District (Mpumalanga Province, South Africa) Using Remote Sensing and GIS. *Can. J. Remote Sens.* **2002**, *28*, 322–327. [CrossRef]
94. Panahi, H.; Azizi, Z.; Kiadaliri, H.; Almodaresi, S.A.; Aghamohamadi, H. Bare Soil Detecting Algorithms in Western Iran Woodlands Using Remote Sensing. *Smart Agric. Technol.* **2024**, *7*, 100429. [CrossRef]
95. Diek, S.; Schaepman, M.E.; De Jong, R. Remote Sensing Creating Multi-Temporal Composites of Airborne Imaging Spectroscopy Data in Support of Digital Soil Mapping. *Remote Sens.* **2016**, *8*, 906. [CrossRef]
96. Polovina, S. Comparison of Methods for Quantifying Erosion Processes Intensity: A Case Study of the Belgrade Master Plan Area. Ph.D. Dissertation, Faculty of Forestry, University of Belgrade, Belgrade, Serbia, 2022. (In Serbian)
97. Carlson, T.N.; Ripley, D.A. On the Relation between NDVI, Fractional Vegetation Cover, and Leaf Area Index. *Remote Sens. Environ.* **1997**, *62*, 241–252. [CrossRef]
98. Gutman, G.; Ignatov, A. The Derivation of the Green Vegetation Fraction from NOAA/AVHRR Data for Use in Numerical Weather Prediction Models. *Int. J. Remote Sens.* **1998**, *19*, 1533–1543. [CrossRef]
99. Congalton, R.G. A Review of Assessing the Accuracy of Classification of Remotely Sensed Data. *Remote Sens. Environ.* **1991**, *37*, 35–46. [CrossRef]
100. Goodchild, M.F.; Guoqing, S.; Ren, Y.S. Development and Test of an Error Model for Categorical Data. *Int. J. Geogr. Inf. Syst.* **1992**, *6*, 87–104. [CrossRef]
101. Paine, D.P.; Kiser, J.D. *Aerial Photography and Image Interpretation*, 2nd ed.; John Wiley, Inc.: New York, NY, USA, 2003.
102. Khorram, S.; van der Wiele, C.F.; Koch, F.H.; Nelson, S.A.C.; Potts, M.D. *Principles of Applied Remote Sensing*; Springer: Cham, Switzerland, 2016; pp. 1–307. [CrossRef]
103. Levin, N. *Fundamentals of Remote Sensing*; Remote Sensing Laboratory, Geography Department, Tel Aviv University: Tel Aviv, Israel, 1999.
104. Tempfli, K.; Huurneman, G.C.; Bakker, W.H.; Janssen, L.L.F.; Feringa, W.F.; Gieske, A.S.M.; Grabmaier, K.A.; Hecker, C.A.; Horn, J.A.; Kerle, N.; et al. *Principles of Remote Sensing: An Introductory Textbook*, 4th ed.; Tempfli, K., Kerle, N., Huurneman, G.C., Janssen, L.L.F., Eds.; International Institute for Geo-Information Science and Earth Observation: Enschede, The Netherlands, 2009; ISBN 978-90-6164-270-1.
105. Radić, B. Erosion as Factor of Landscape Degradation in Serbian Ski-Resorts. Ph.D. Dissertation, Faculty of Forestry, University of Belgrade, Belgrade, Serbia, 2014. (In Serbian)
106. Dobrota, M.M. Statistički Pristup Definisanju Zone Osetljivosti u Metodama Daljinskog Uzorkovanja (A Statistical Approach to Sensitivity Zone Definition in Remote Sensing Methods). Ph.D. Dissertation, Faculty of Organizational Sciences, University of Belgrade, Belgrade, Serbia, 2018. (In Serbian)
107. Abdi, A.M. Land Cover and Land Use Classification Performance of Machine Learning Algorithms in a Boreal Landscape Using Sentinel-2 Data. *GIScience Remote Sens.* **2020**, *57*, 1–20. [CrossRef]
108. Cohen, J. A Coefficient of Agreement for Nominal Scales. *Educ. Psychol. Meas.* **1960**, *20*, 37–46. [CrossRef]
109. Landis, J.R.; Koch, G.G. The Measurement of Observer Agreement for Categorical Data. *Biometrics* **1977**, *33*, 159. [CrossRef]
110. Olofsson, P.; Foody, G.M.; Herold, M.; Stehman, S.V.; Woodcock, C.E.; Wulder, M.A. Good Practices for Estimating Area and Assessing Accuracy of Land Change. *Remote Sens. Environ.* **2014**, *148*, 42–57. [CrossRef]
111. R Core Team. R: The R Project for Statistical Computing. Available online: https://www.r-project.org/ (accessed on 19 March 2024).